Comparison of Direct and Inverse Model-based Disturbance Observer for a Servo Drive System

Nándor Fink, Guo Zenan, Péter Szemes, Péter Korondi

Department of Mechatronics, Faculty of Engineering, University of Debrecen,
Ótemető u. 2-4, 4028 Debrecen, Hungary
fink.nandor@eng.unideb.hu; guozenan@eng.unideb.hu;
szemespeter@eng.unideb.hu; korondi.peter@eng.unideb.hu

Abstract: The well-known disturbance observer – which is based on the transfer function of the inverse model –, was published almost four decades ago. To practically implement the inverse of the transfer function a filter is added to it, in order to eliminate high frequency disturbance signals. A key step of the design of this Inverse Model Based Disturbance Observer (IMBDO) is the selection of the filter with appropriate parameters. This paper proposes a disturbance observer, which is based on direct model (DMBDO) and it can work without any additional filter. It simplifies the design and the implemented controller code. Discrete time implementations of IMBDO and DMBDO are compared by a simple internet-based servo system in a non-real-time control environment. The effect of non-equidistant sampling is examined.

Keywords: friction compensation; servo drive system; discontinuous control friction compensation

1 Introduction

In the field of motion control, the elimination of disturbance is a key task. Disturbance source could be the effect of external load variation, parameter changes due to aging and friction due to operational conditions. This paper focuses on the non-linear, time invariant effect of friction.

In most cases making the proper model of the disturbance is ineffective or impossible. The disturbance elimination method based on the estimation of the disturbance is widely used. In [1] [2] [3] an observer-based control was applied for rehabilitation purposes, in [4] a long-distance laser positioning was carried out using DOB (Disturbance Observer) method, in [5] [6] the complex and changing environment justified the choice of using a DOB based control, in [7] the lack of sensory data was bridged with a DOB control. It is also used for the motion control of drones [8], for telemanipulation systems [9] [10] [11] and for other disturbance

rejection purposes [12] [13] [14] [15]. A specific type of neural network called long short-term memory (LSTM) recurrent neural network to identify the system behavior in real-time [16]. A method that uses a specific type of filter called a discrete Kalman filter to estimate the behavior of the system while being robust to small disturbances [17]. A combination of two different estimation techniques, an Extended Kalman filter and a Takagi-Sugeno fuzzy observer, to estimate the behavior of a strip winding system [18].

The idea of the estimation of the disturbance has a long history, it was already used in 1983 [19]. A guide for the design of the disturbance observer was stated in [20] [21].

The motivation for using either the inverse or direct modeling approach in disturbance observers is to improve the performance of the control system in the presence of disturbance [41]. These two methods could estimate the disturbance signal accurately and substract it from the measured output to obtain a better estimate of the output. Direct model based disturbance observer is easier to model the system dynamics directly, rather than computing the inverse model. The direct model can provide predictions of the system response, which can eliminate the signal frequency and estimate the disturbance signal. Despite the DOB control being a robust method, it also has its limits [22] [23] [24] [25]. In [26] an improved method has been shown for disturbance rejection (based on DOB), because the to-be-controlled system had too much uncertainty for the traditional DOB. Other problems that exceeds the boundaries of the classical method are stated in [27] [28]. In [29], it describes a study on modeling of observation in cognitive process, it discusses different aspects of the observation with perception and attention. The multicomponent fixed-point iteration is a specific type of mathematical iterative in adaptive control of a univariate second-order system in [30]. A new method for modeling tower crane systems using tensor product-based model transformation is proposed in [31]. A soft computing-based disturbance observer is published in [32] and a sliding mode-based disturbance observer is proposed in [33]. In [34] experiments were performed with an electro-hydraulic actuator controlled by a neural network sliding mode control method, where an Extended State Observer (ESO) was used for noise estimation and rejection with impressive results. Applying DOB for stochastic systems is in [35], and applying for the fractional-order system is in [36]. The ADRC (Active Disturbance Rejection Control) method is examined in [37] [38], and an overview of DOB robust control was presented in [39]. In [40] a signal was decomposed to seven components with different frequency bands with dual-tree complex wavelet transform (DTCWT) method, and each component was noise reduced based on a singular value decomposition (SVD) method. Basic methods and applications of the disturbance observer-based control are presented in [41]. The comparison of PID and sliding mode controller in the teaching field and internet-based control is shown in [42] [43]. Compared with other works, this paper presents a method without a filter to the inverse disturbance observer can eliminate high-frequency interference signals. The motivation of this

paper is to propose a direct model without a filter, simplifying the design steps and the code of the control.

The structure of the paper will be the following. After the introduction, the second section summarizes the mathematical foundations of disturbance observers. The third section presents the experimental setup used in the measurement. The fourth section compares the measurement results. The robustness is discussed in this section too. Finally, the fifth section draws the most important conclusions of the article.

2 Brief Overview of the Mathematical Bases of Disturbance Estimators

2.1 Inverse Model-based Disturbance Observer (IMBDO)

The simplified motor model is described by (1) (2) [41] where the input and output are noted by u and y, respectively. Since the actual real values of the model parameters are not known, the nominal parameters T_n and G_n are used in the inverse model. The d is the disturbance signal at the input and it is estimated by $\hat{d}$.

$$y(s) = \frac{G_m}{1 + sT_M}\big(u(s) + d(s)\big) \tag{1}$$

$$d = \frac{1 + sT_m}{G_m}y - u \qquad \hat{d} = \frac{1 + sT_n}{G_n}y - u \tag{2}$$

Fig. 1 shows the principal operation of a very simple disturbance observer described by (2). The upper part is a simplified diagram of a motor modeled by a mechanical time constant T_m and a gain G_m, while the lower part is the disturbance estimator, which is the inverse of the motor model.

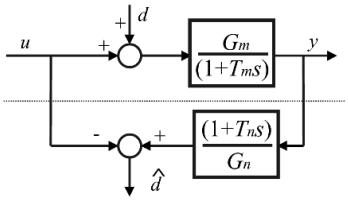

Figure 1
Simple Inverse Model Based Disturbance Observer, IMBDO

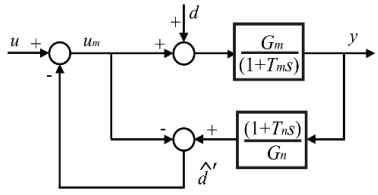

Figure 2
Simple Inverse Model Based Disturbance Observer with feedback

The differences between the nominal and the real system model are considered parameter perturbation, which can be formulated as follows.

$$T_m = T_n + \Delta T_n \qquad G_m = G_n + \Delta G_n \tag{1}$$

ΔT_n and ΔG_n are limited. It can be seen that the estimated disturbance signal, $\hat{d}$ (indicated in Fig. 1) contains not only the value of the real disturbance signal, but also carries information about the deviation of the parameters (3). The effect of the disturbance signal d can be compensated by feedback on the estimated disturbance signal $\hat{d}$ (see Fig. 2).

After simple calculations, it follows that from the input u to the output signal y the transfer function is $G_n/(1 + T_n s)$ in Figure 2, and y does not depend on the disturbance signal.

In practice, a pure differentiating term can be a serious problem as it amplifies the noise. The effect of noise amplification can be eliminated by the low-pass filter $W(s)$ in the feedback branch, as shown in Figure 3.

The cutoff frequency of $W(s)$ must be much higher than the reciprocal of the dominant time constant T_m of the servo system (so that the useful signal is not filtered out), in the meantime it must be small enough to suppress the measurement noise sufficiently. Of course, a low-pass filter $W(s)$ can be combined with the inverse of the system model and they should be realized together. (see Figure 4).

The absolute value of the transfer function of the disturbance signal to y can be sufficiently small in the lower frequency range if $W(s)$ is properly designed. This method can be generalized, but even then the problem remains that most controlled plants are integrative in nature, so the inverse will be derivative in nature.

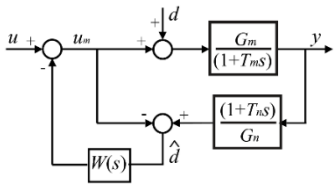

Figure 3
Simple Inverse Model Based Disturbance Observer with feedback and filter

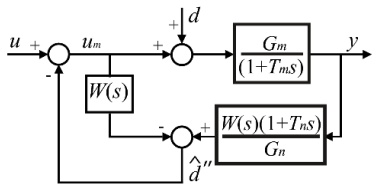

Figure 4
Simple Inverse Model Based Disturbance Observer with feedback and distributed filter

Possible time delay is an additional problem. In the late 1990s, a multitude of articles addressed how to design a $W(s)$ filter that provides optimal operation over a wide range. In summary, the biggest problem with this method is that it is based on the inverse model. The disturbance observer with inverse model has a strong connection in the real world application in [44] [45].

2.2 Direct Model-based Disturbance Observer (DMBDO)

Hereinafter, we again consider the same simple motor model (1) with the same parameter perturbation (3) as in the case of IMBDO. The principle is very simple, the difference between the output signals of the ideal and the perturbed model y_e is fed back to the perturbed model with a sufficiently high gain (Figure 5).

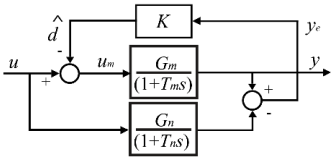

Figure 5
Direct Model Based Disturbance Observer

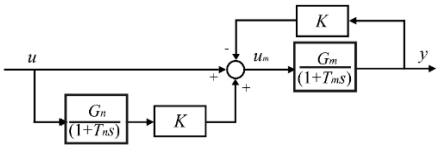

Figure 6
Redrawn direct model based disturbance observer

If K is large enough, then the difference between the two signals y_e must be smallso that the feedback signal $\hat{d}$ is not too large, which means that the feedback signal $\hat{d}$ contains information about the parameter uncertainties ΔT_n and ΔG_n. To calculate the transfer function from u to y, Figure 5 must be redrawn as shown in. According to Figure 6, the transfer function input u and output y using the l'Hospital rule:

$$\lim_{K\to\infty}\left(\left(1+\frac{KG_n}{1+sT_n}\right)\frac{\frac{G_m}{1+sT_m}}{1+K\frac{G_m}{1+sT_m}}\right)=\lim_{K\to\infty}\left(\frac{1+sT_n+G_nK}{1+sT_n}\,\frac{G_m}{sT_m+KG_m+1}\right)=$$

$$=\lim_{K\to\infty}\left(\frac{\frac{1+sT_n}{K}+G_n}{1+sT_n}\,\frac{G_m}{\frac{1+sT_m}{K}+G_m}\right)=\frac{G_n}{1+sT_n} \tag{2}$$

Similarly to Figure 1, add limited disturbance $d(t)$ to the input of the perturbed controlled plant (see Figure 7).

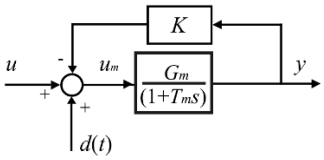

Figure 7
Disturbance rejection part of direct model based disturbance observer

Effect of disturbance $d(t)$ on the output:

$$\lim_{K\to\infty}\left(\frac{\frac{G_m}{1+sT_m}}{1+K\frac{G_m}{1+sT_m}}\right)=0 \tag{3}$$

This can be interpreted as meaning that the feedback signal $\hat{d}$ in Figure 6 carries information about both limited parameter uncertainty and limited input disturbance. The method can be generalized to multi-input, and multi-output systems as well.

2.3 Relay as an Approximation of Infinity Gain

Let us substitute gain K by a simple relay with a relay gain G_r.

$$\hat{d} = G_r sign(y_e) \tag{4}$$

The robustness of the disturbance rejection method is due to its large (ideally infinitely large) gain. This is ensured by a relay in the feedback branch. The gain can be defined by the ratio of the output and input signals. As the error tends to zero the gain tends to be infinite.

$$K = \lim_{y_e \to 0} \frac{G_r sign(y_e)}{y_e} = \infty \tag{5}$$

From the point of view of practical application, the biggest advantage of the relay control law (6) is that it can be easily implemented even with a simple analog operational amplifier, therefore a relatively high switching frequency can be achieved, and it can directly control power electronics semiconductor switching elements. Therefore, it can also be used where the maximum time constant of the controlled plant is relatively small (below ms) and where rapid control is required and the hardware used is not suitable for performing complex calculations between two samples. In contrast, the disadvantage is that it cannot provide for the high gain in the entire state space. There are two conflicting expectations about the value of G_r. The higher the value of G_r, the larger the range of the state space it can provide high gain, but at the same time it can result in a larger chattering around the ideal output signal. The disturbance rejection control method is widely used in the real world application, such as process control system, mechatronics systema and flight control system [41].

3 Experimental System

3.1 The Hardware Description

The system components are listed in Tab. 1 and a photo is presented in Figure 8. The data flow is shown in Figure 9.

Pulses from the incremental encoder that is attached to the permanent magnet DC motor (4) are sent to the computer via the interface circuit (2) and data acquisition card (1). The torque reference signal is transmitted from the computer to the motor controller (5) via the data acquisition card (1) and via the interface circuit (2).

The current signal of the DC motor (4) is sent to the motor controller (5) via the interface circuit (2) and PWM voltage signal returns to the servo motor (4). The source of the power is the ATX power supply (3). The disc (7) is connected to the DC motor shaft via a clutch as a load and the rotation of the disc can be monitored during the measurement using the webcam (6).

Table 1

Parts of the experimental system

Nr.	Element	Type
1	Data acquisition (Counter and DA card)	Advantech USB-4704
2	Interface circuit	ASIC
3	ATX Power supply	ATX 12V GPS-500A8
4	DC Motor with incremental encoder	maxon A-max 110075, MR, Type M, 512 CPT
5	Motor controller unit	maxon
6	Webcamera	USB 2.0 Logitech C525
7	Aluminum disc load	Custom made

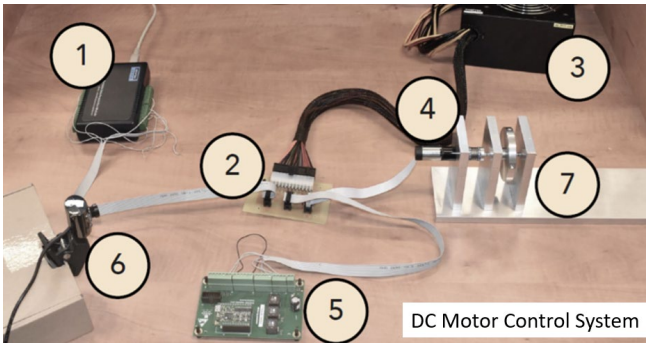

Figure 8

Photo of the experimental setup

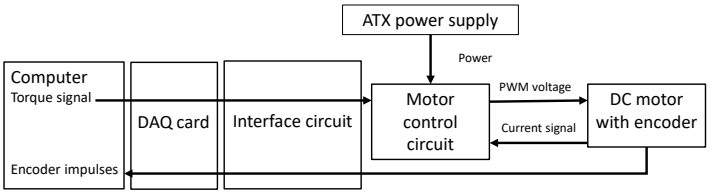

Figure 9

The signal and data flow

3.2 System Equations

3.2.1 Reference Model

The reference model is calculated online as a result of system identification measurement, which is part of the controller application. The discrete time $W_{dm}(z)$ transfer function is calculated first, where the input is the torque $M_m(z)$ and the output is the velocity $\omega(z)$.

$$W_{dm}(z) = \frac{\omega(z)}{M_m(z)} = \frac{0.06}{z - 0.6} T_s = 2\ ms, \tag{6}$$

where T_s is the sampling time of the experimental system. The continuous transfer function $W_{cm}(s)$ can be calculated from (8)

$$W_{cm}(s) = \frac{\omega(s)}{M_m(s)} = \frac{0.15}{0.004s + 1} \tag{7}$$

In contrast to, the simplified model (8) and (9), a detailed model of the servo system is used in the Simulink simulation as described in the following section. The disturbance signal d contains three effects: i.e. friction models, un-modelled dynamics and parameter perturbation.

3.2.2 Model of the Servo System

The goal of the simulation is to tune the parameters of the proposed disturbance observer, a simplified model is used which includes every challenging elements: un-modeled dynamics, the friction model, parameter perturbation and velocity saturation as shown in Figure 10.

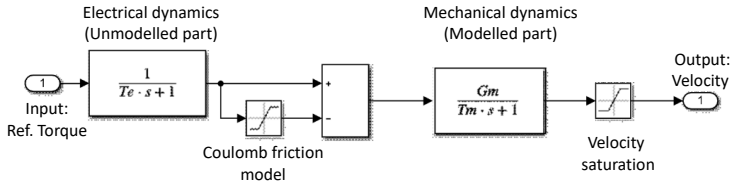

Figure 10
Simulink model of the motor

The input of this system model is the reference torque calculated by the disturbance observer. The torque is measured in perunit %. $T_e = 0.1\ ms$ represents electric dynamics (including the electric time constant of the motor and the current control loop), which is unmodelled from the point of view of the disturbance observer design. The output of unmodelled electric part is the electric torque of the motor. The torque effect of Coulomb friction is modeled by saturation. If the absolute value of the motor is smaller than $T_{rc} = 11\%$ then it is set to zero. The simulated ω_{sim} and the measured ω_{meas} velocities are compared in Figure 11.

The effect of Stribeck friction (what was approximated as Coulomb friction model in Fig. 10), is clearly seen as a time shifted signal in case of measured curve ω_{meas}. The static friction is bigger than the moving friction and there is hysteresis effect as well, which is why unlike ω_{sim}, the first quarter period of ω_{meas} cannot be mirrored to obtain its second quarter. The accurate modeling of the friction is out of the scope of this paper. This simplified (Coulomb) friction model is satisfactory from the point of view of parameter setting. A more detailed friction model of this system is published in [43]. $T_m = 23\ ms$ is the mechanical time constant and $G_m = 0.7$ is the gain. The parameter uncertainties are quite big $\Delta T_m = -19\ ms$ and $\Delta G_m = -0.55$. They are around 80%. The output velocity is saturated $\omega_{max} = 11\ rad/s$ as well. The time constants are read from the data sheet of the motor. The values of G_m, T_{rC} and the offset is identified by measurement shown in Figure 11. The Stribeck effect is ignored in this model since all differences between the real system and the reference model are considered disturbance which we try to reduce.

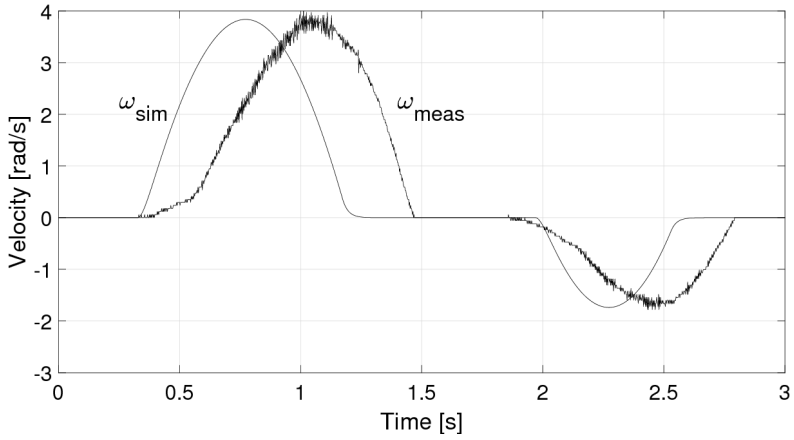

Figure 11
Comparison of simulated and measured velocity

The goal is to change the original dynamic of the servo system and force it to follow the reference model by disturbance rejection method. Let us use the following first-order reference model in the time domain.

$$J_r \dot{\omega}(t) = u_m(t) - B_r \omega(t) \tag{10}$$

where J_r is the inertia and B_r is the constant of the viscous friction of the reference model. u_m is the input electric torque. Parameters of the applied simplified model shown in Figure 10 are calculated from (10).

$$T_m = \frac{J_r}{B_r} \quad G_m = \frac{T_{rmax}}{100 J_r} \tag{11}$$

The simulation parameters are summarised in Table 2.

Table 2
Simulation parameters

Torque reference			
Amplitude=20 and 40		$T_p = 3$	$offset = 1.5$
Time constants			
$T_e = 0.0001$	$T_S = 0.002$	$T_m = 0.002$	$T_1 = T_2 = 0.002$
Gains			
$G_m = 0.7$		$G_r = 0.6$	
Saturations			
$\omega_{max} = 11$		$T_{rC} = 11$	
Parameter perturbation			
$\Delta T_m = -0.019$		$\Delta G_m = -0.55$	

3.2.3 Inverse Model-based Disturbance Estimation and Compensation

The theory of the inverse model based is typically developed in continuous time, as it is based on the mathematical model that describes the system's behavior over time. However, the implementation of the method is often done in discrete time practically, as most real-world systems are controllers using digital controllers that operate on discrete-time signals. The discrete-time version of the idea presented in Figure 4, is implemented. The Simulink model of the system with a disturbance observer is shown in Figure 12.

The sampling method is modeled by a zero-order holder. The lower part of the figure is the disturbance observer. The filters are applied. The first one for the modified input torque signal u_m is the discrete time version of a second order low pass filter given in (12).

$$W_f(s) = \frac{1}{(1 + sT_1)(1 + sT_2)} \tag{12}$$

The filter for the velocity signal is a multiplication of (12) and the inverse of the reference model (9).

$$W_f(s) = \frac{1}{(1 + sT_1)(1 + sT_2)} \tag{13}$$

$$W_{fx}(s) = \frac{0.004s + 1}{0.15(1 + sT_1)(1 + sT_2)} \tag{14}$$

A key step of the design is the selection T_1 and T_2. The time constants of the filter are set between the sampling time and the mechanical time constant.

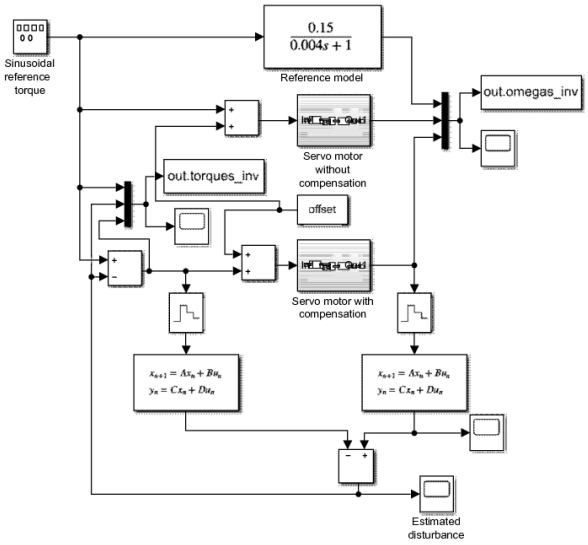

Figure 12
Simulink model of a common IMBDO

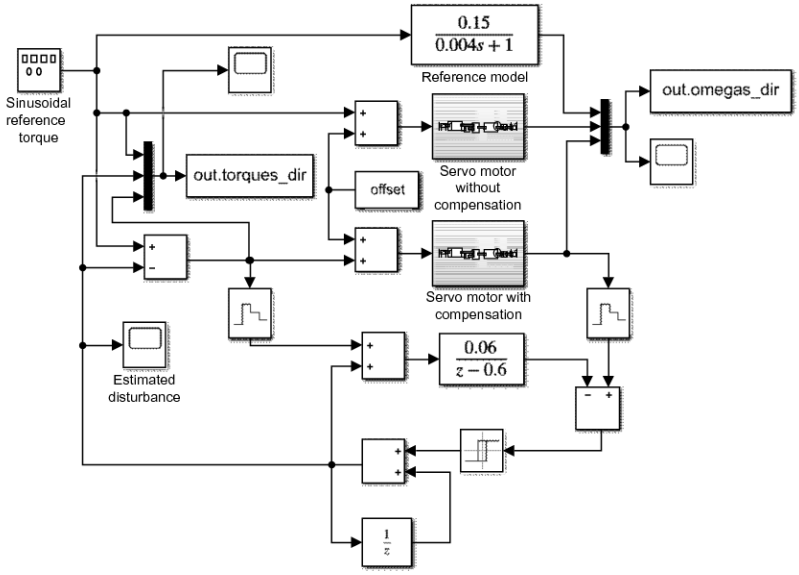

Figure 13
Simulink model of the proposed DMBDO

3.2.4 Direct Model-based Disturbance Estimation and Compensation

Since the estimated disturbance signal $\hat{d}$ is the output of the relay it has a high frequency component, which might cause chattering in the ω. On one hand, we need a small relay gain G_r as possible to reduce the chattering effect, on the other hand G_r must be big enough to cover the disturbance ($G_r > \hat{d}_{max}$). If $\hat{d}(t)$ is a continuous and limited function than the change of disturbance in one sampling period $\Delta\hat{d}(t)$ is also limited and only this change must be covered by the rely upon the discrete time application.

$$\hat{d}[k] = \hat{d}[k-1] + G_r sign(y_e) \tag{15}$$

3.3 Simulation Results

The main challenge is friction compensation. Two sets of measurement results are presented. The u inputs are sinusoidal in all cases in this paper. From the physical point of view, u is the torque reference signal, which is given in perunit percentage. First, the amplitude of u is 20%. The control loop of the armature current is realized by an operational amplifier, which has an uncompensated offset. The actual acceleration torque is shifted in the positive direction vertically. The offset of the operational amplifier causes asymmetrical non-compensated velocity ω_{nc} as shown in Figure 14, when the disturbance observer is switched off.

When the sinusoidal input torque u is smaller than the static friction torque, the motor cannot move ω_{nc} (due to Stribeck friction). The real motor movement starts around 0.1 s and the velocity increases faster than the ideal ω_{id} velocity. The motor stops again when the motion friction torque becomes bigger than the real motor torque.

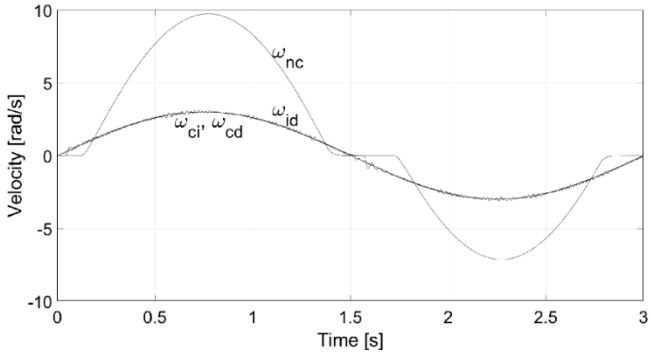

Figure 14
Velocities (u_{max}=20%)

The three velocities (calculated by the ideal model ω_{id}, by IMBDO ω_{ci} and by DMBDO ω_{cd}) are seems quite similar in Figure 14. To show the differences, the phenomenon around zero-crossing is magnified in Figure 15.

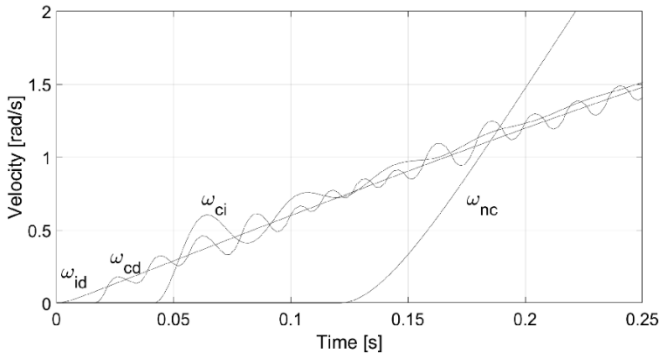

Figure 15
Velocities around zero-crossing (u_{max}=20%)

The response of DMBDO is faster but ω_{cd} has a continuous oscillation around ω_{id}. In case of IMBDO, ω_{ci} there is a kind of overshoot around zero-crossing and it has a very small constant error. The faster response of DMBDO is visible in Figure 16 and Figure 17 as well.

The Coulomb friction (as an approximation of Stribeck effect) changes its sign at zero-crossing of velocity signal so the disturbance observer must follow this change. The estimated disturbance of DMBDO $\hat{d}(t)_{cd}$ follows the Coulomb friction faster than $\hat{d}(t)_{ci}$ of IMBDO. Because of the offset the positive and negative half periods are asymmetrical. It explains the shape of the estimated disturbance signals $\hat{d}(t)_{ci}$ and $\hat{d}(t)_{cd}$ in Figure 16 and Figure 17.

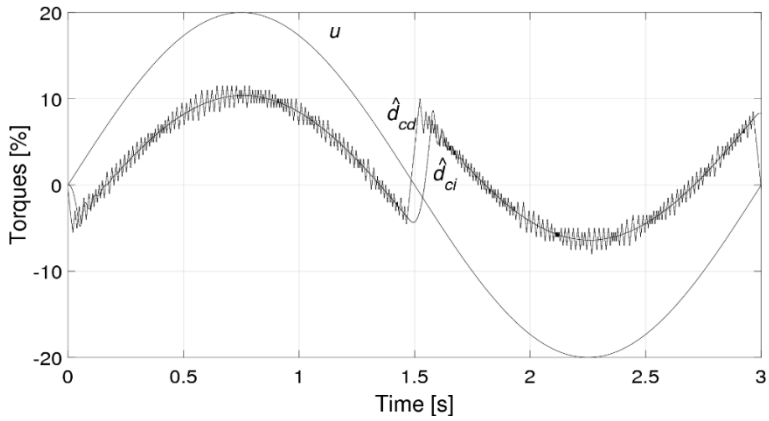

Figure 16
Torques (u_{max}=20%)

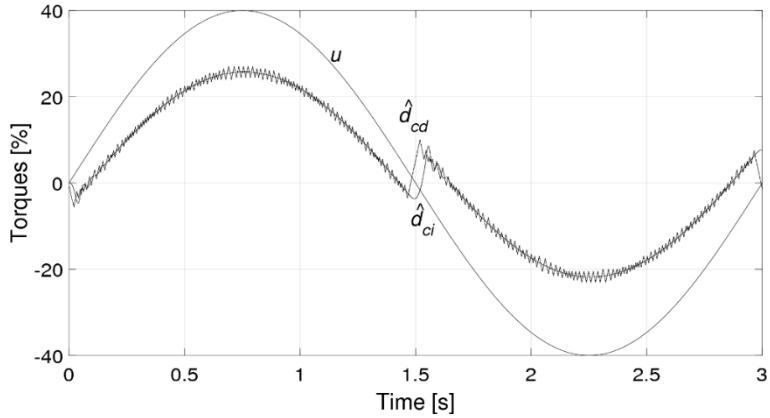

Figure 17
Torques (u_{max}=40%)

If the amplitude of the reference torque is 40% the non-compensated velocity ω_{nc} is saturated at the maximum velocity of the motor as shown in Figure 18. Because of the offset the saturation is longer in the positive half period than that in the negative half period.

4 Measurement Results

The experimental results are quite similar to that of simulation in the previous chapter. Since the real motor shaft velocity is calculated from the impulses of the incremental encoder it is quite noisy. First $u_m = 20\%$ is set. In most cases the measured noise is bigger than the difference between the two methods as shown in Figure 19 and Figure 20.

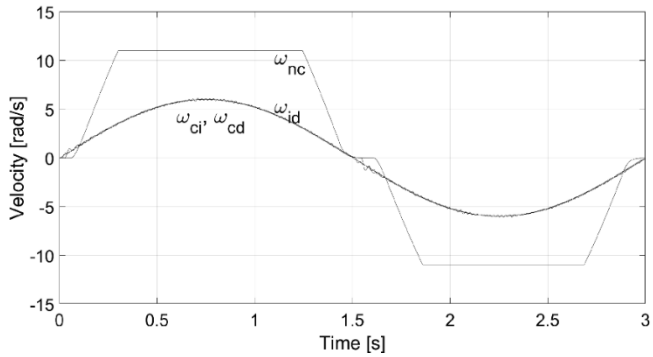

Figure 18
Velocities (u_{max}=40%)

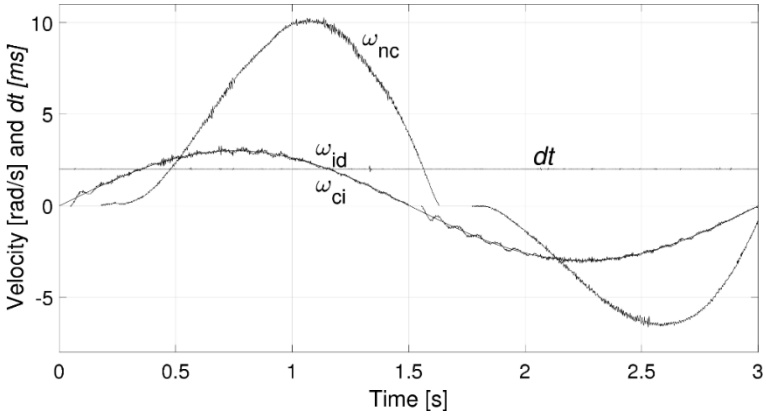

Figure 19
Velocities of IMBDO (u_{max}=20%)

The main challenge is the non-equidistant sampling. The applied operating system is a general purpose, not a real-time operating system, and accurate sampling cannot be ensured. Usually, the sampling delay is less than 0.2 ms, but sometimes the time difference between two samplings can be 20 times bigger than the intended $T_s = 2\ ms$. Figure 23 shows one of the worst periods (peaks in the figure) detected during the measurements. The distribution of length is shown in Figure 24.

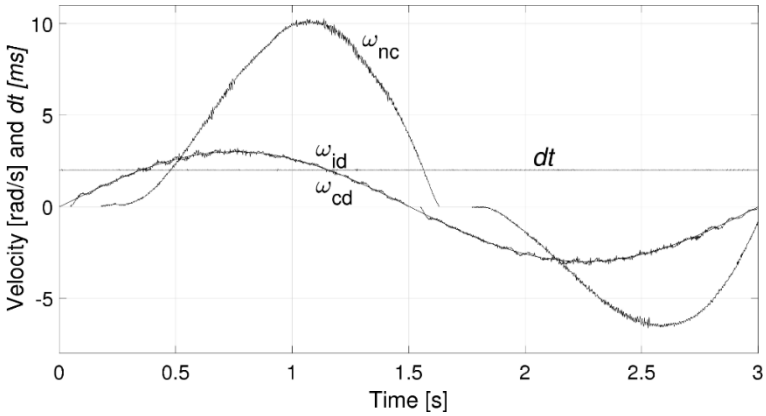

Figure 20
Velocities of DMBDO (u_{max}=20%)

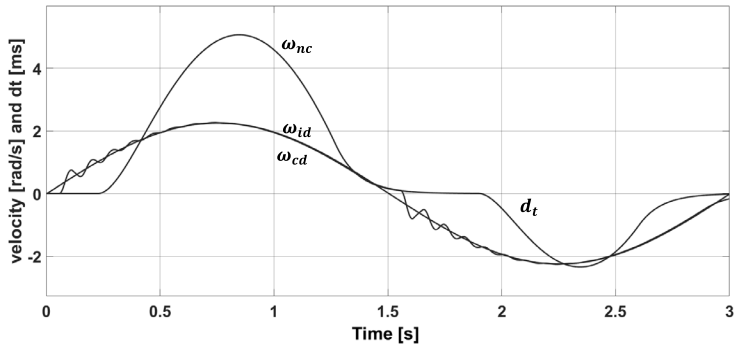

Figure 21
Velocities of IMBDO (u_{max} =15%)

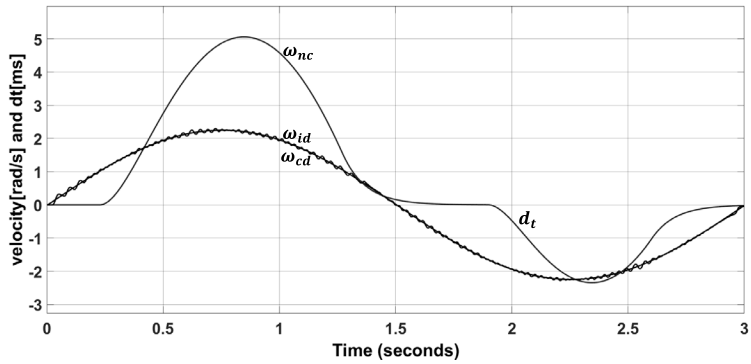

Figure 22
Velocities of DMBDO (u_{max} =15%)

Figure 21 and Figure 22 show another velocity comparison of IMBDO and DMBDO with the u_{max} =15%. It depicts that the DMBDO without the filter has nearly the same performance compared with the IMBDO. The Servo motor with compensation reduces the chattering with the u_{max} increasing. DMBDO has the same trajectory but better performance than IMBDO under the same parameters.

Figure 19 and Figure 21 depict that the velocity with the compensation could converge to the reference velocity in a finite time. The velocity response is steady, but when the velocity crosses the horizontal line it has an oscillation. Compared with the IMBDO, the velocity with compensation in DMBDO converges to the reference in a finite time, and the velocity in DMBDO has a more steady performance than the velocity in IMBDO (Figure 20 and Figure 22).

Time-variant sampling periods cause oscillation, which has a bigger amplitude in case of IMBDO, ω_{ci} than in case of DMBDO, ω_{cd}. The system operated for 5 minutes (100 periods) and the worst periods are selected in both cases. The results are shown in Figure 25 and Figure 26. As it was anticipated from Figure 15, the performance of DMBDO is a little bit better than that of IMBDO.

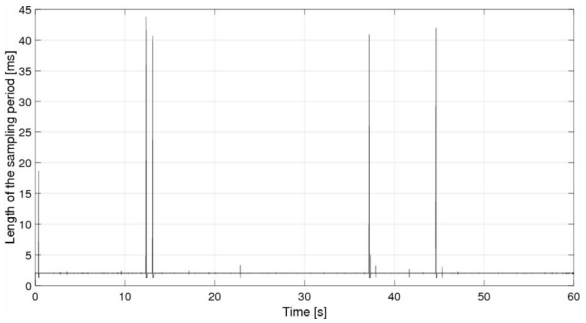

Figure 23
The length of the sample period

Finally, the case of $u_m = 40\%$ is measured as shown in Fig. 25 and Fig. 26. The Stribeck effect (as a time shifted signal) is clearly seen again. The zero-crossing is plotted in Figure 29. Similarly to Figure 15, the delay of the movement is shorter and the amplitude of oscillation is smaller in the case of DMBDO, ω_{cd}.

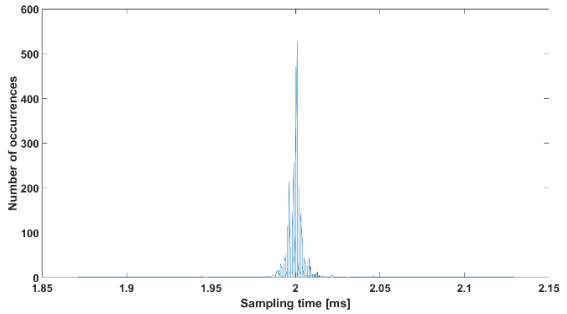

Figure 24
Distribution of length of the sampling periods

The theory of the direct disturbance observer and inverse disturbance observer is usually developed in continuous time because they are based on a mathematical model describing the behavior of the system over time. But the real implementation of the method is usually performed in discrete time because most real-world systems are controlled using digital controllers operating on discrete-time signals.

5 Control Code Robustness Analysis

IMBDO and DMBDO have a low sensitivity to the variations in the parameters of the controller plant and disturbance as a robust control method. Since the input signal u is determined by a relay it is pulse width modulated. The mean value of the torque u can be influenced by changing the duty ratio. The reason for the robustness is that the switching frequency of the torque reference signal is 500 Hz.

The response of the system to a change in load can be less than 2 ms. Let us compare the sampling time with the system time constant. According to the motor data sheet, the mechanical time constant is $T_m = 23\ ms$, which is an order of magnitude larger than the sampling time, so that the controller can react faster than the change would appear in the motion state. The other important question is how long it takes for the digitally calculated input signal u to convert to physical torque. The non-modeled dynamics of the armature coil and current control loop, which can be characterized by the electric time constant $T_e = 0.1\ ms$, plays a decisive role in this. It can be stated that the input signal used in our model changes at least one order of magnitude faster than the sampling time. Comparing Fig. 19 to Figure 20 and Figure 27 to Figure 28, it can be seen that there is no significant difference between the ideal ω_{id}, the compensated ω_{ci} and ω_{cd} velocity signals if the actual sampling periods are close to $T_s = 2ms$.

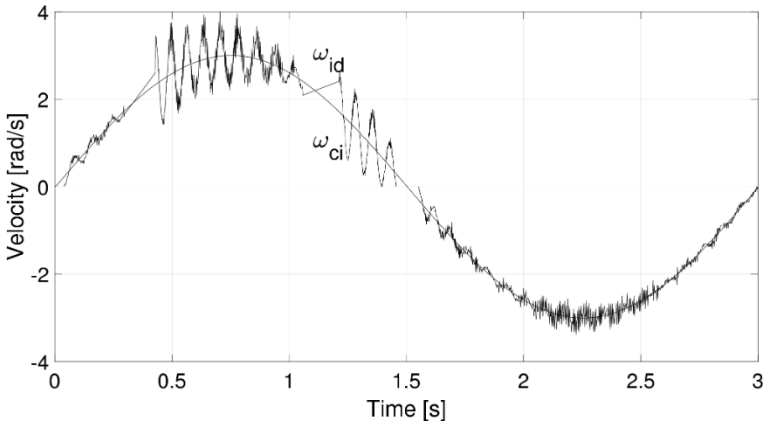

Figure 25
Velocities of IMBDO (u_{max}=20%)

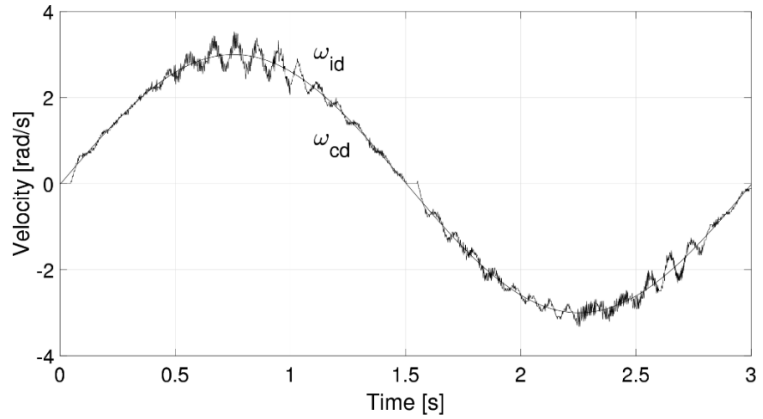

Figure 26
Velocities of DMBDO (u_{max}=20%)

Table 3
Comparison of time constants of the system

Times		
Actuator delay	***Sampling time***	***Dominant time constant***
$T_e = 0.1\ ms$	$T_s = 2\ ms$	$T_n = 23\ ms$

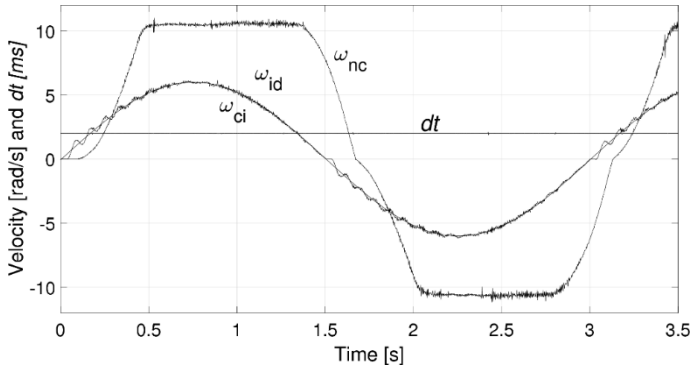

Figure 27
Velocities of IMBDO (u_{max}=40%)

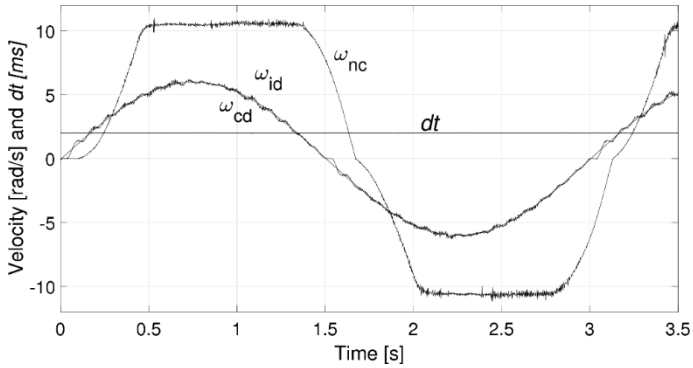

Figure 28
Velocities of DMBDO (u_{max}=40%)

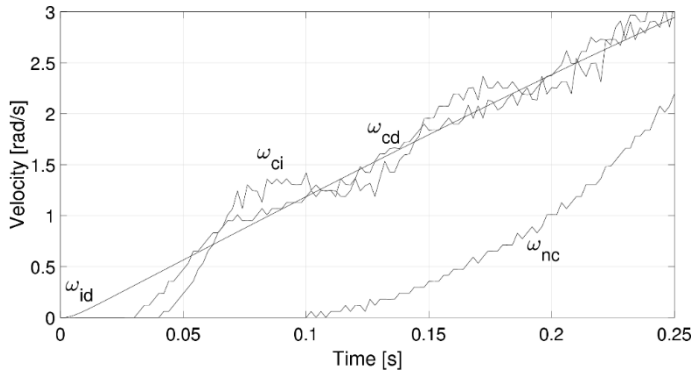

Figure 29
Zero-crossing of DMBDO and IMDBO (umax=40%)

Conclusion

A discrete time Inverse Model Based Disturbance Observer (IMBDO) and a Direct Model Based Disturbance Observer (DMBDO) are implemented as a simplified, non-real-time controller-based servo system. The performance of the two types of disturbance observers is compared by simulation and experiments. The DMBDO has some advantages to IMBDO in this particular, servo control application. The implementation of DMBDO is simpler since the filter is not needed, in case of model inversion. The design is easier and the resulting controller code is also simpler and more robust. Case of practical code implementation the execution time of the controller (also the computational complexity of the) algorithm is shorter, which can be important in case of low cost (i.e. microcontroller) applications. DMBDO can respond faster to the sudden change of the disturbance and it is less sensitive to non-equidistant sampling. It means it can be used in a non real-time environment, as especially in the education system.

Acknowledgement

The project TKP2020-NKA-04 has been implemented with the support provided by the National Research, Development and Innovation Fund of Hungary, financed under the 2020-4.1.1-TKP2020 funding scheme.

The authors wish to thank the support of the Hungarian Research Fund (OTKA K143595).

References

[1] Mohammadi A. and Dallali H. Disturbance observer applications in rehabilitation robotics: an overview., 2020, pp. 113-133, doi:10.1016/B978-0-12-817450-0.00005-5

[2] Saadatzi M. N., Poshtan J., and Saadatzi M. S. Application of mimo disturbance observer to control of an electric wheelchair using nsga-ii. Journal of Medical Signals and Sensors, 2011, 1(2) pp. 122-129

[3] Brahmi B., Driscoll M., El Bojairami I. K., Saad M., and Brahmi A. Novel adaptive impedance control for exoskeleton robot for rehabilitation using a nonlinear time-delay disturbance observer. ISA Transactions, 2021, pp. 108:381-392, doi:10.1016/j.isatra.2020.08.036

[4] Deng J., Xue W., Zho X., and Mao J. On disturbance rejection control for inertial stabilization of long-distance laser positioning with movable platform. MEASUREMENT AND CONTROL, 2020, 53(7-8) pp. 1203-1217, doi:10.1177/0020294020935492

[5] He L., Xiong C.-H., Zhang Q.-H., Chen W.-B., Fu C.-L., and Lee K.-M. A backpack minimizing the vertical acceleration of the load improves the economy of human walking. IEEE Trans Neural Syst Rehabil Eng., 2020, 28(9) pp. 1994-2004, doi:10.1109/TNSRE.2020.3011974

[6] Ming L. and Heping L. Disturbance observer-based variable structure control on the working attitude balance mechanism of underwater robot., 2009, 1 pp. 232-237, doi:10.1109/ICCET.2009.202

[7] Surapong N. and Mitsantisuk C. Position and force control of the scara robot based on disturbance observer. Procedia Computer Science, 2016, 86 pp. 116-119, doi:10.1016/j.procs.2016.05.029

[8] Sasaki K. and Yang Z.-J. Disturbance observer-based control of uavs with prescribed performance. INTERNATIONAL JOURNAL OF SYSTEMS SCIENCE, 2020, 51(5) pp. 939-957, doi:10.1080/00207721.2020.1746436

[9] Sun D., Liao Q., Stoyanov T., Kiselev A., and Loutfi A. Bilateral telerobotic system using type-2 fuzzy neural network based moving horizon estimation force observer for enhancement of environmental force compliance and human perception. Automatica, 2019, 106 pp. 358-373, doi:10.1016/j.automatica.2019.04.033

[10] Singh H., Panzirsch M., and Ryu J.-H. Preserving the physical coupling in teleoperation despite time delay through observerbased gradient control. IFAC-PapersOnLine, 2019, 52(18) pp. 25-30, doi:10.1016/j.ifacol.2019.12.201

[11] Coutinho F. and Cortes˜ao R. Online stiffness estimation for robotic tasks with force observers. Control Engineering Practice, 2014, 24 pp. 92-105, doi:10.1016/j.conengprac.2013.11.002

[12] Sakow M. Novel robust disturbance observer. ISA Transactions, 2020, 104 pp. 255-277, doi:10.1016/j.isatra.2020.05.023

[13] Tao Z., Shu W., Lei W., and Yang Z. Active disturbance rejection control of servo systems with friction., 2009, pp. 558-561, doi:10.1109/CASE.2009.119

[14] Ding K. and Zhu Q. Extended dissipative anti-disturbance control for delayed switched singular semi-markovian jump systems with multi-

disturbance via disturbance observer. Automatica, 2021, p. 128, doi:10.1016/j.automatica.2021.109556

[15] Wang L., Freeman C. T., Rogers E., and Young P. Disturbance observer based repetitive control system with non-minimal state space realization and anti-windup mechanism. IFAC-PapersOnLine, 2020, 53(2) pp. 1505-1510, doi:10.1016/j.ifacol.2020.12.2008

[16] Christudas, F, and Angeline V. D. "System identification using long short term memory recurrent neural networks for real time conical tank system." Rom. J. Inf. Sci. Technol 23 (2020): 57-77

[17] Volovyk, A. Yu, V. M. Kychak, and D. V. Havrilov. "Discrete Kalman Filter Invariant to Perturbations." Acta Polytechnica Hungarica 18, No. 10 (2021): 21-41

[18] Szedlak-Stinean, A. I., Precup, R. E., Petriu, E. M., Roman, R. C., Hedrea, E. L. and Bojan-Dragos, C. A., 2022, Extended Kalman filter and Takagi-Sugeno fuzzy observer for a strip winding system. Expert Systems with Applications, 208, p.118215

[19] Ohishi, K. and Ohnishi, K.and Miyachi, K. Torque-speed regulation of dc motor based on load torque estimation. Proc. IEEJ IPEC-TOKYO, 1983, 2 pp. 1209-1216

[20] Sariyildiz E. and Ohnishi K. A guide to design disturbance observer. J. Dyn. Sys., Meas., Control., 2013, 136(2) pp. 021011-1-021011-10, doi:10.1115/1.4025801

[21] Chen W.-H. Disturbance observer based control for nonlinear systems. IEEE/ASME TRANSACTIONS ON MECHATRONICS, 2004, 9(4) pp. 706-710, doi:10.1109/TMECH.2004.839034

[22] Sariyildiz E. and Ohnishi K. Analysis the robustness of control systems based on disturbance observer. International Journal of Control, 2013, 86(10) pp. 1733-1743, doi:10.1080/00207179.2013.795663

[23] Shim H. and Jo N. H. An almost necessary and sufficient condition for robust stability of closed-loop systems with disturbance observer. Automatica, 2009, 45(1) pp. 296-299, doi:10.1016/j.automatica.2008.10.009

[24] Choi Y., Yang K., Chung W. K., Kim H. R., and Suh I. H. On the robustness and performance of disturbance observers for second-order systems. IEEE TRANSACTIONS ON AUTOMATIC CONTROL, 2003, 48(2) pp. 315-320, doi:10.1109/TAC.2002.808491

[25] Oboe R. How disturbance observer changed my life., 2018, pp. 13-20, doi:10.1109/AMC.2019.8371055

[26] Qiu Z., Hu S., and Liang X. Disturbance observer based adaptive model predictive control for uncalibrated visual servoing in constrained

environments. ISA Transactions, 2020, pp. 106:40-50, doi:10.1016/j.isatra.2020.06.013

[27] Chen J., Sun R., and Zhu B. Disturbance observer-based control for small nonlinear uav systems with transient performance constraint. Aerospace Science and Technology, 2020, p.105, doi:10.1016/j.ast.2020.106028

[28] Wen X., Sun Y., Wang J., and Yao X. Rejection of timevarying frequency sinusoidal disturbance using refined observer for a class of uncertain systems. ISA Transactions, 2020, 100 pp. 136-144, doi:10.1016/j.isatra.2019.11.039

[29] Pozna, C. and Precup, R. E., 2012, Aspects concerning the observation process modelling in the framework of cognition processes. Acta Polytechnica Hungarica, 9(1), pp.203-223

[30] Redjimi, H. and Tar, J. K., 2021, Multiple Components Fixed Point Iteration in the Adaptive Control of Single Variable 2nd Order Systems. Acta Polytechnica Hungarica, 18(9), pp.69-84

[31] Hedrea, E. L., Precup, R. E., Roman, R. C. and Petriu, E. M., 2021, Tensor product-based model transformation approach to tower crane systems modeling. asian journal of control, 23(3), pp.1313-1323

[32] Raul-Cristian Roman, Radu-Emil Precup, and Emil Petriu. Hybrid data-driven fuzzy active disturbance rejection control for tower crane systems. EUROPEAN JOURNAL OF CONTROL, 2020, 58 pp. 373-387, doi:10.1016/j.ejcon.2020.08.001

[33] P. Korondi, K. D. Young, and H. Hashimoto. Sliding mode based disturbance observer for motion control., 1998, pp. 1926-1927

[34] Wending L., Guanglin S., Chun Z., Hongyu L., and Junyong F. RBF Neural Network Sliding Mode Control Method Based on Backstepping for an Electro-hydraulic Actuator. Strojnĭski vestnik - Journal of Mechanical Engineering, 2020, 66(12) pp. 697-708, doi:10.5545/sv-jme.2020.6866

[35] Wei X.-J.,Wu Z.-J., and Karimi H. R. Disturbance observer-based disturbance attenuation control for a class of stochastic systems. Automatica, 2016, 63 pp. 21-25, doi:10.1016/j.automatica.2015.10.019

[36] Liu R., She J., Zhu F., and Nie Z. Robust disturbance rejection for a fractional-order system based on equivalent-input-disturbance approach. Science China Information Sciences, 2018, 61 pp. 1-12, doi:10.1007/s11432-017-9368

[37] Han J. From pid to active disturbance rejection control. IEEE Trans. Ind. Electron., 2009, 56(3) pp. 900-906, doi:10.1109/TIE.2008.2011621

[38] Cortes-Romero J., Delgado-Aguilera E., and Jimenez-Triana A. Robust fractional active disturbance rejection control: A unified approach. ISA Transactions, 2020, 107 pp. 63-77, doi:10.1016/j.isatra.2020.08.003

[39] Sariyildiz E., Obor R., Ohnishi K., and Fellow L. Disturbance observer based robust control and its applications: 35th anniversary overview. IEEE TRANSACTIONS ON INDUSTRIAL ELECTRONICS, 2020, 67(3) pp. 2042-2053, doi:10.1109/TIE.2019.2903752

[40] Xihui C., Gang C., Ning L., Xinhui S., and Wei L. Research on a Noise Reduction Method Based on DTCWT, and the cyclic singular energy difference spectrum. Strojniˇski vestnik - Journal of Mechanical Engineering, 2020, 66(10) pp. 613-626, doi:10.5545/sv-jme.2020.6704

[41] Li, Shihua, Jun Yang, Wen-Hua Chen, and Xisong Chen. Disturbance observer-based control: methods and applications. CRC press, 2014

[42] Zenan, G., Szemes, P.T. and Korondi, P., 2022, October. Bond graph-based teaching method to enhance the synergy of mechatronics in Lab VIEW. In 2022 IEEE 9th International Conference on e-Learning in Industrial Electronics (ICELIE) (pp. 1-6) IEEE

[43] Róbert, M., Balázs, S., Dobák, D. and Tamás, S. P., 2022, September. Internet Based Control of a Servo Motor with a Sliding Mode Based Observer for Chattering Reduction. In 2022 IEEE 20th International Power Electronics and Motion Control Conference (PEMC) (pp. 209-215) IEEE

[44] Güvenç, B.A., Güvenç, L. and Karaman, S., 2010, Robust MIMO disturbance observer analysis and design with application to active car steering. International Journal of Robust and Nonlinear Control: IFAC-Affiliated Journal, 20(8), pp. 873-891

[45] Chan, S. P., 1995, A disturbance observer for robot manipulators with application to electronic components assembly. IEEE Transactions on Industrial Electronics, 42(5), pp. 487-493

[46] Gróf, P ; Takarics, B ; Petres, Z ; Korondi, P., Tensor product model type polytopic decomposition of a pneumatic system with friction phenomena taken into account., In: IEEE - IEEE (szerk.) 2010 IEEE 8th International Symposium on Applied Machine Intelligence and Informatics New York (NY), Amerikai Egyesült Államok: IEEE (2010) pp. 153-158, Paper: 5423747, 6 p. doi: 10.1109%2FSAMI.2010.5423747